Characterizing Non-linearities in the Chandra LETG+HRC-S Dispersion Relation

Sun Mi Chung[a], Jeremy J. Drake[a], Vinay L. Kashyap[a], Peter W. Ratzlaff[a] and Bradford J. Wargelin[a]

[a]Chandra X-ray Center, Harvard-Smithsonian Center for Astrophysics, 60 Garden St, Cambridge, MA 02138

ABSTRACT

The Chandra Low Energy Transmission Grating Spectrometer (LETGS) is comprised of 3 micro-channel plate (MCP) segments and is primarily used with the High Resolution Camera spectroscopic array (HRC-S). In-flight calibration data observed with the LETG+HRC-S show that there are non-linear deviations in the positions of some lines by as much as 0.1 Å. These deviations are thought to be caused by spatial non-linearities in the imaging characteristics of the HRC-S detector. Here, we present the methods we used to characterize the non-linearities of the dispersion relation across the central plate of the HRC-S, and empirical corrections which greatly reduce the observed non-linearities by a factor of 2 or more on the central MCP.

Keywords:

1. INTRODUCTION

There are two transmission gratings onboard the Chandra X-ray Observatory—the High Energy Transmission Grating (HETG) and the Low Energy Transmission Grating (LETG). The Low Energy Transmission Grating Spectrometer (LETGS) (Brinkman et al. 2000) consists of the LETG and the High Resolution Mirror Assembly (HRMA) and one of two focal-plane imaging detectors. The LETG is primarily used with the High Resolution Camera spectroscopic array (HRC-S). The LETG+HRC-S covers the wavelength range of 1.2 to 170 Å in the positive and negative orders, with a dispersion of 1.148 Å/mm.

In an earlier paper (Chung et al. 2004) we described problems with the observed dispersion relation, as discovered from in-flight calibration data. Data showed that the outer HRC-S plates required a larger value of the Rowland diameter than what was needed for the central plate. In addition, systematic non-linear deviations of up to ∼0.05 Å in the positions of many spectral lines across all three HRC-S plates were observed, as compared to accurate theoretical or laboratory wavelengths. In this paper, we will discuss further improvements to the dispersion relation of the LETG+HRC-S combination.

Errors in the dispersion relation of up to 0.05 Å can be quite significant to the interpretation of data. Non-linearities in the dispersion relation not only limit the accuracy of the determination of the centroid of a line, but also broaden the observed line profiles. At a wavelength of 150 Å, an error of 0.05 Å corresponds to a velocity of 100 km s^{-1}, which is typical of non-thermal motions in astrophysical sources such as stellar coronae and is similar to the equatorial velocities of rapidly rotating X-ray bright stars such as AB Dor (Schmitt et al. 1997).

In the limit of perfect imaging characteristics, the accuracy of the determination of the centroid of a narrow (ie at or close to the instrumental width) spectral line is in principle limited only by signal-to-noise ratio. For many spectral lines seen in astrophysical sources, sufficient counts are acquired that this limit is much smaller than 0.05 Å. Moreover, the instrument appears stable with a drift over the period of a given astrophysical observation (typically about 100 ks) of only 0.01 Å or less. We are therefore strongly motivated to improve the dominant source of wavelength error. We demonstrate below that this originates in the imaging system, the HRC-S microchannel plate detector.

First we describe the observations which were used in our study of the LETG dispersion relation, then we discuss our methods of analysis to probe the imaging distortions and apply empirical corrections to the data. Finally, we discuss the improvements that have been made with our empirical corrections, as well as future plans to further improve the non-linearities of the dispersion relation.

Further author information: Send correspondence to J.J.D.: E-mail: jdrake@cfa.harvard.edu

UV and Gamma-Ray Space Telescope Systems, edited by
Günther Hasinger, Martin J. L. Turner, Proceedings of SPIE Vol. 5488
(SPIE, Bellingham, WA, 2004) · 0277-786X/04/$15 · doi: 10.1117/12.552194

2. OBSERVATIONS

Observations used for the analyses described in this paper are listed in Table 1. Standard Chandra Interactive Analysis of Observations (CIAO) pipeline-processed data were downloaded from the Chandra public data archive.*

Table 1. Observations used in our analyses.

Target Name	ObsID	Exposure [ks]	Start Date	offset [arcmin]
α Aur	1248	85.23	1999 Nov 9 13:27:21	0
α Aur	2582	28.83	2002 Oct 4 23:57:53	-1.5
α Aur	3479	30.38	2002 Oct 6 10:01:58	1.5
V4743 Sgr	3775	25.07	2003 Mar 19 09:29:09	0

The data listed in Table 1 have all been uniformly reprocessed following the CIAO thread on LETG+HRC-S grating analysis † In addition to applying the standard grating analysis CIAO thread, we have also included a correction that removes the constant wavelength offset observed between the central and outer HRC-S plates. This offset is due to errors in the effective gap sizes between the micro-channel plates in the software model (Chung et al. 2004). Our correction has since been incorporated into the CIAO software system.

All of the data utilized in our analyses were observed with Normal Mode Pointing (NMP). For observations made with NMP, the Chandra telescope dithers in a Lissajous pattern, which distributes the photons across multiple detector elements. The amplitude of the dither is 40 $\times$ 40 arcseconds, which spans approximately 300 HRC-S pixels (6.43 μm square) in both the dispersion and cross-dispersion directions. We can take advantage of the dither pattern in order to compare the non-linearities of the dispersion relation at different locations on the detector.

The primary source that was used in our analyses was α Aur (Capella). Capella is an evolved active binary with an emission line spectrum comprised of many bright and narrow lines arising from transitions in highly ionised astrophysically abundant elements (e.g. O, Ne, Mg, Si, S, Fe etc), mostly in the range 5-25 Å, but also including a handful of useful features at longer wavelengths. It is the brightest object of this class in the X-ray sky and is therefore a good target for our calibration analyses which involve cross-correlating spectra and comparing the positions of narrow lines with accurately known theoretical or laboratory wavelengths. Two of the Capella observations used in our analyses have aimpoints which are off-set along the dispersion axis by $\pm$1.5 arcminutes. These off-set observations allow us to probe the HRC-S imaging distortions along a greater range of the dispersion axis because they place bright, strong lines on different detector locations. We also used data from a bright nova, V4743 Sagittarii, to test whether the wavelength corrections we derived from Capella improve the non-linearities of the dispersion relation observed in sources other than Capella. V4743 Sgr exhibits a complex and rich absorption line spectrum in the range of $\sim$20 to 50 ÅẆhile the individual lines of the V4743 Sgr spectrum are not so useful for determining line centroids and comparing them to absolute line wavelengths, the spectrum of this bright nova is quite good for analysis with the cross-correlation technique described in section 3.3.1 below.

3. ANALYSIS

3.1. Dispersion Relation

The dispersion relation of the LETGS is calibrated and monitored through observations of cosmic sources with well-understood emission features. In principle, there is only one variable to calibrate: the spectrograph Rowland diameter. This can be obtained by the standard grating equation and the comparison of the positions of observed features with their theoretical or laboratory wavelengths.

*http://asc.harvard.edu/cda

†http://asc.harvard.edu/ciao/threads/spectra_letghrcs

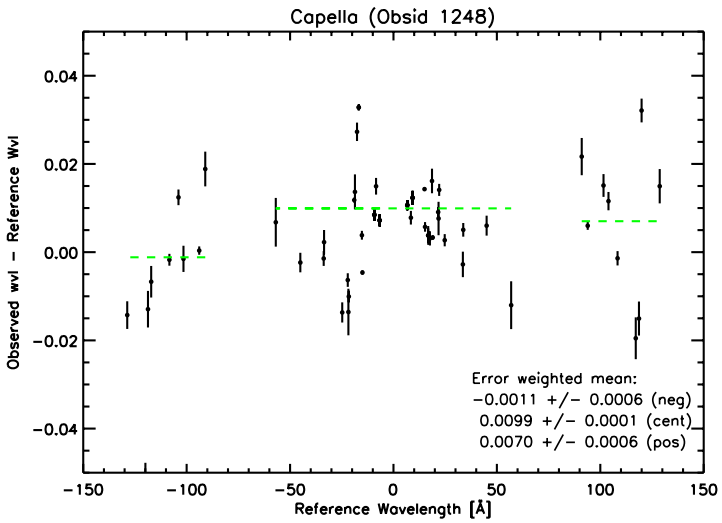

Figure 1. The dispersion relation of Capella Obsid 1248, for standard processed data (after adjustment of plate gap sizes in the software model). The dashed line indicates the error-weighted mean of the difference between the observed and reference line wavelengths for data on each of the three HRC-S plates. Note that the error-weighted means are significantly off-set from zero because of the non-linearities of the dispersion relation.

The HRC-S detector (Zombeck et al.1995) is a CsI coated microchannel plate design with approximate dimensions 300×20 mm, where the long axis corresponds to the dispersion axis. The HRC-S is split into three microchannel plate segments, each approximately 100 mm long. Soon after launch, it was discovered that the Rowland diameter derived from the observed spectral features on the outer HRC-S plates is slightly larger by 0.05% than the Rowland diameter derived from data on the central plate ($\lambda \leq 0$Å). It was later revealed that this was due to numerical errors in processing software (Chung et al. 2004).

The dispersion relation also showed a significant constant wavelength offset between the central and outer plates of the detector. This wavelength discontinuity was attributed to errors in the effective sizes of the gaps between microchannel plates. A correction was applied to all our data by enlarging the plate gaps between the central and outer plates by 8.7 and 3.8 pixels (S1 and S3 plates, respectively).

Figure 1 shows the dispersion relation for Capella data which has been reprocessed with the enlarged plate gaps. (See Chung et al. 2004 for dispersion relation of data before plate gaps were enlarged). Although there are prominent non-linearities, the RMS across the entire wavelength range shown is only 0.014 Å. The RMS across just the central plate is 0.012 Å. Note the non-linear residuals between the measured line wavelengths and the theoretical or laboratory wavelengths.

3.2. Spectral lines trailed by spacecraft dither

One very direct way to characterize the non-linearities of the dispersion relation is to look at the photon events of a bright line in a coordinate system defined by the observed line wavelength, λ, and the dispersion axis of the detector, referred to as `tdety` in the Chandra coordinate system. Figure 2 shows the event list data of Capella (ObsID 1248) in λ versus `tdety` space. The horizontal width that the photons span across `tdety` is approximately 300 pixels, which is determined by the size of the dither pattern projected onto the `tdety` axis. The photon events of the Fe XVII emission line shown in this figure "wobble" across the detector in a very non-linear fashion. We can actually see the spatial non-linearities of the detector by looking at data in this way. If the dispersion relation were perfectly flat, the photons in Figure 2 would line up in a horizontal straight line across `tdety`.

We can then map out the non-linearities of the dispersion relation along the dispersion axis by determining the wavelength centroid of events as a function of `tdety`. To do this, photon events for each spectral line are

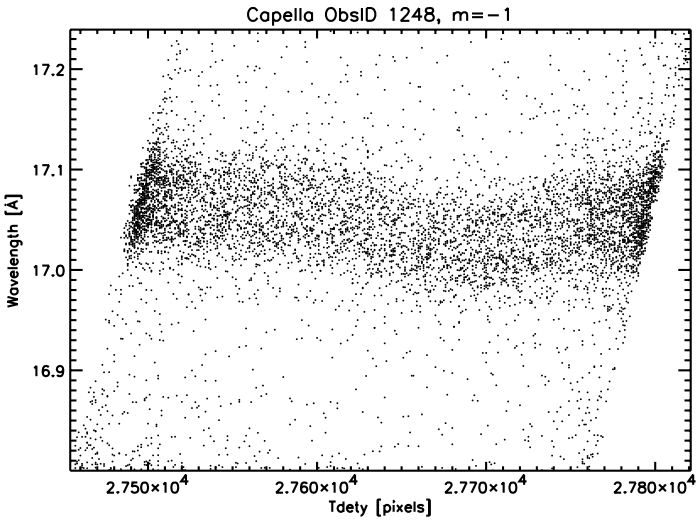

Figure 2. Event list data of Fe XVII emission line from Capella ObsID 1248, negative order, in λ versus `tdety` coordinates, for standard processed data. Note that the photon events wobble across the detector non-linearly.

split up into bins of `tdety` and histograms are computed for each bin as a function of wavelength. The number of `tdety` bins are varied for each line so as to maintain an approximately constant S/N ratio for data in all bins. Modified Lorentzian functions of the form $F(\lambda) = a/(1 + \frac{\lambda-\lambda_0}{\Gamma})^\beta$ are then fit to these histograms in order to obtain the observed wavelength centroids (Figure 2), where a is the amplitude and Γ is a characteristic line width, with a value of 2.5 for β. The modified Lorentzian function with a value of 2.5 for β has been shown to provide a good match to LETG+HRC-S line profiles (Drake et al. 2003). In this way, we map out the observed line wavelengths as a function of `tdety`. Comparison of these wavelengths with the line reference wavelengths then yeilds the detector distortion as a function of `tdety`. The final aim is to combine these distortions for a number of lines in order to map them out over as large an area of the detector as possible.

The drawback to this analysis is that it only works for relatively strong emission lines for which there are sufficient counts to accurately measure the wavelength centroids as a function of `tdety`. The area of the detector over which we can realistically map out the distortions is therefore limited. While weaker lines can be useful, they cannot be split into fine `tdety` bins and therefore result in lower effective resolving power for mapping out the detector distortions.

Figure 3 illustrates the difference between observed and theoretical wavelengths as a function of the detector dispersion axis, `tdety`, as obtained from the analysis described above. In black circles we show results obtained from Capella ObsID 1248, and in gray circles we show the combined results of ObsID 1248 and also the two off-set Capella observations (ObsIDs 2582 and 3479). A spline is fit through the data points and smoothed by 3 pixels. The smoothed splines are shown as the black and gray curves. Notice that Figure 3 only shows a wavelength range of 0-40Å. Although we do have a few wavelength centroids measured from lines on the outer HRC-S plates, most of the strong lines fall on the central plate. Therefore, in this paper we concentrate on developing an empirical correction for dispersion relation non-linearities on the central plate only.

The smoothed splines are used as an empirical wavelength correction by simply subtracting off the correction from the observed wavelength of each photon event, based on its `tdety` location.

3.3. Post-Correction

Figure 4 shows the original negative order event list data of Capella ObsID 1248 in gray and the corrected data in black. We can see there is a clear improvement in the non-linearity. The wavelength corrected events are now in a much straighter line across `tdety` and do not "wobble" as significantly across the dispersion axis.

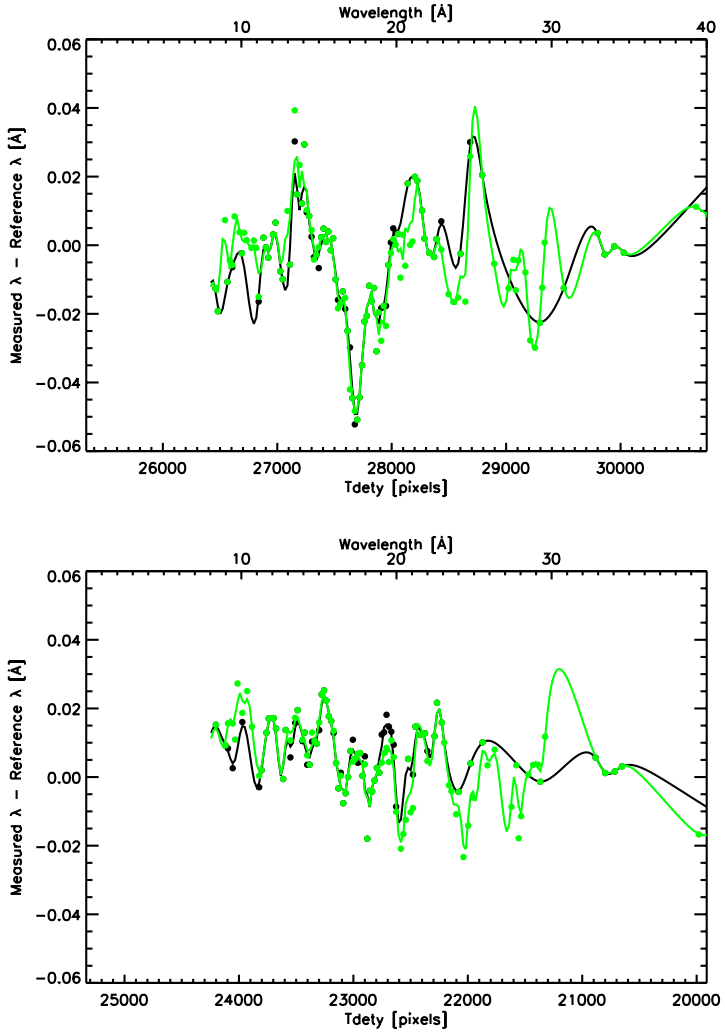

Figure 3. Measured minus reference wavelengths as a function of the detector dispersion axis `tdety` for the wavelength range of 0-40 Å. We fit a spline to the data points (circles) and smoothed the spline by a few pixels. Results obtained from the analysis of Capella ObsID 1248 are shown in black, and those obtained from Capella ObsIDs 1248, and the two off-set pointings (ObsIDs 2582 and 3479), are shown in gray. The black smoothed spline was used as the wavelength correction for ObsID 1248, and the gray smoothed spline was used as the correction for ObsID 3775.

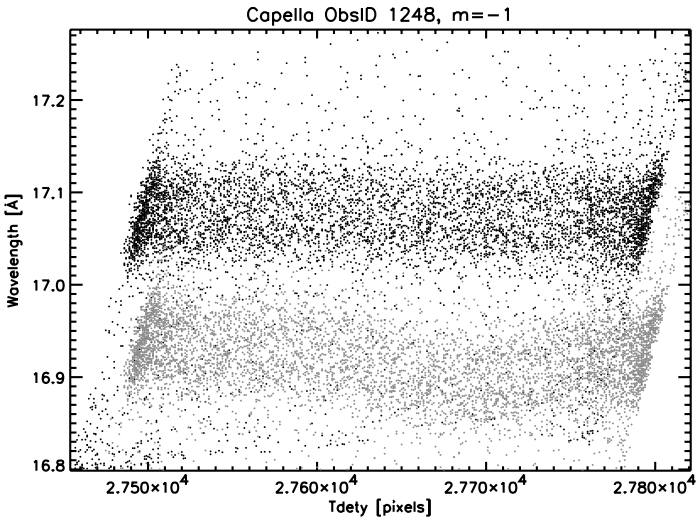

Figure 4. Event list data of Fe XVII emission line from Capella ObsID 1248, negative order, in λ versus `tdety` coordinates. In gray we show the original data, which has been arbitrarily offset in the vertical direction for sake of clarity. The photons of this emission line are dispersed non-linearly across the detector. In black we show the corrected data, which has now flattened out and forms a straighter line across the detector.

Figure 5 also shows line profiles for the negative order of the original data and the wavelength corrected data. The wavelength corrected data show line profiles that are less broadened and have sharper peaks.

Figure 6 shows the dispersion relation for Capella data after it empirical wavelength corrections have been applied. The dispersion relation on the central plate shows significant improvement. Although there are still what appear to be systematic non-linearities in the dispersion relation of the central plate, the RMS has decreased from 0.012 Å to a mere 0.0045 Å, an improvement of nearly a factor of three.

3.3.1. Cross-correlation

Another way we can characterize the non-linearities of the dispersion relation is to cross-correlate spectra which are extracted from photon events that land on different areas of the detector. In order to extract spectra from events that correspond to different detector locations for a given wavelength, we split up the dither pattern into four regions in the dispersion direction. We used time filters based on the observatory pointing aspect telemetry to split events by dither location. The "dither-split" spectra were then extracted from these time-filtered event lists by using the CIAO tool `tgextract`. We then cross-correlate spectra that are extracted from the event lists of the middle two "dither-split" regions (ie, events of any given wavelength are separated by $\sim$75 pixels). Cross-correlation of these two spectra provides a useful diagnostic in characterizing the relative wavelength shifts between different detector regions.

When cross-correlating the two spectra, we designate one spectrum as the 'reference', to which the second spectrum is compared. By shifting one spectrum relative to the reference spectrum, and computing a correlation coefficient at each shift, we can determine at which wavelength difference $\delta\lambda$ the two spectra are best matched. There are various ways of computing such a correlation signal. In our case, we have computed the χ^2 value at each shift:

$$\chi^2 = \sum \frac{(C_{ref}(\lambda) - C_2(\lambda+\delta\lambda))^2}{\sigma_{ref}(\lambda)^2 + \sigma_2(\lambda+\delta\lambda)^2}; \quad \lambda - \Delta\lambda \leq \lambda \leq \lambda + \Delta\lambda \tag{1}$$

where $C_{ref}(\lambda)$ and $C_2(\lambda+\delta\lambda)$ are the two spectra being compared, in the form of counts/0.0125 Å, and $\sigma_{ref}(\lambda)$ and $\sigma_2(\lambda+\delta\lambda)$ are the respective errors. These quantities are then summed over a window region. The parameter $\delta\lambda$ represents the offset between the two spectra at which the test statistic is computed, and $\Delta\lambda$ is the wavelength interval over which the spectra are compared. This last parameter needs to be sufficiently large that enough

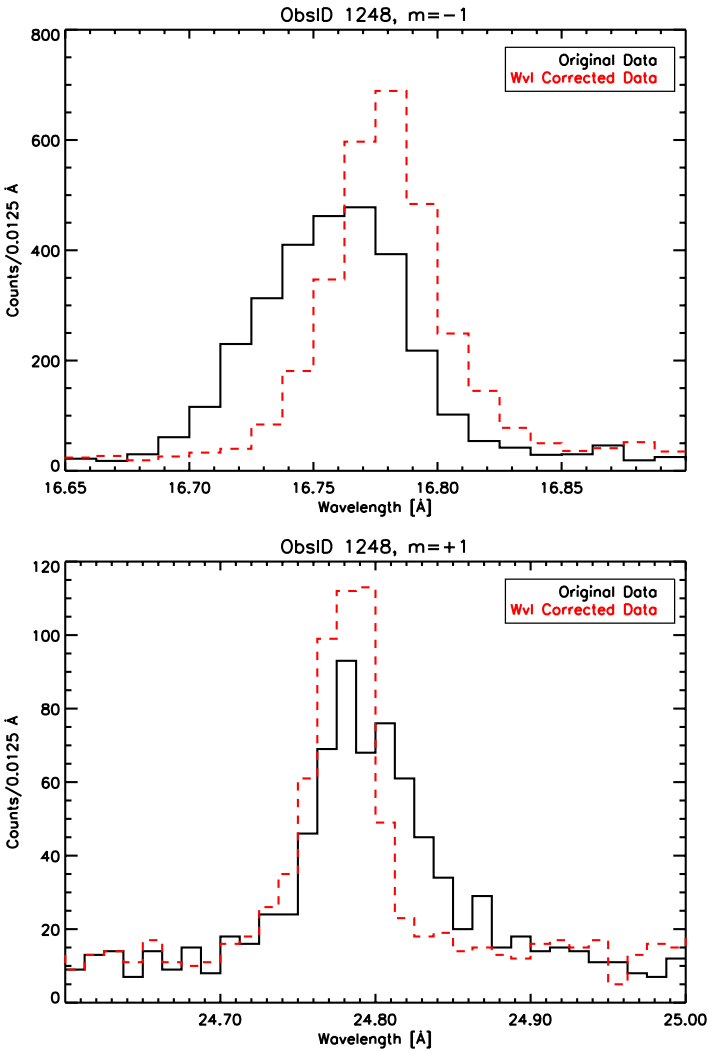

Figure 5. Line profiles of standard processed Capella data (solid) versus line profiles of data with empirical wavelength correction applied (dashed), for negative (top) and positive (bottom) orders. In both plots, the data that have been corrected have narrower widths and sharper, more well-defined peaks. Notice that the wavelength centroids of these profiles have also shifted.

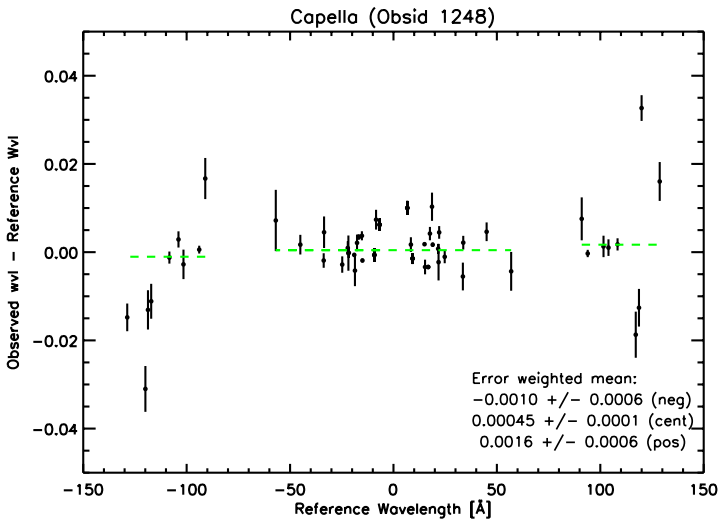

Figure 6. The dispersion relation of Capella Obsid 1248, after empirical wavelength corrections were applied. Error-weighted means for each MCP is indicated by a dashed line. In comparison to Figure 1, the non-linearities of the data on the central plate have been significantly reduced.

signal is included, but sufficiently small so as to usefully probe the scale size of the distortions. Typically, we have adopted a value of 0.6 Å, and computed χ^2 at intervals of 0.003 Å. We use the Gehrels approximation to estimate the errors on the observed counts in the spectra.

In order to obtain the uncertainty on the value of $\delta\lambda$ that corresponds to the minimum χ^2, we have utilized a Monte-Carlo method in which we obtain random realizations of the spectra $C_2(\lambda)$ N number of times, (where $N \sim 10 - 20$), and cross-correlate the reference spectrum with each of the randomized data sets. The 1σ uncertainty on the magnitude of the distortion is then the standard deviation of the distribution of the minima that is produced.

Figure 7 shows the results from the cross-correlation analysis for the original data (black) and the wavelength corrected data (gray), in the wavelength range of 0-40Å. The top panel of each plot shows the relative distortions of Capella data (ObsID 1248), and the bottom panel shows relative distortions of the V4743 Sgr data (ObsID 3775). The error bars for the Capella data tend to be smaller than those for the V4743 Sgr data because Capella has higher S/N and sharper features. The relative distortions flatten out significantly once the empirical wavelength corrections have been applied. Although in a few places, the magnitude of the distortion does get worse, there is a large overall improvement, particularly at the very short wavelengths $\leq$20Å.

4. FUTURE WORK

Although we have significantly improved some of the observed non-linearities on the central plate, the distortions on the outer plates still need to be corrected, as do those on some remaining parts of the central plate lacking useful diagnostic in-flight data at this time. We await more data that will allow us to map out the distortions in these detector regions and thereby implement a more complete correction for the dispersion relation non-linearities.

We are working to devise a method that will allow us to infer the distortions in detector regions where high S/N lines are absent. This might be accomplished by utilizing information from the cross-correlation analysis (which provides information about the *r*elative distortions) and combining this with the absolute distortions obtained from centroiding high S/N lines along `tdety`.

The problem of detector imaging non-linearities is closely linked with the detector "degap" correction. The HRC is a position-sensitive charge detector comprised of one axis of parallel wires, and another axis of gold

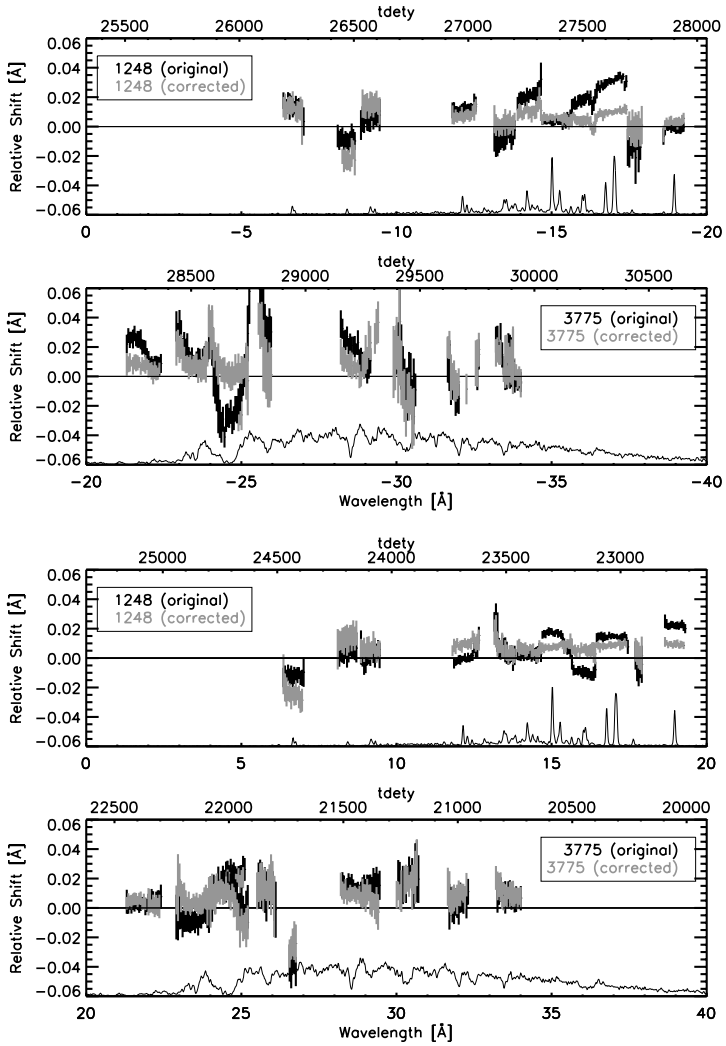

Figure 7. Relative wavelength shifts obtained by cross-correlating spectra extracted from different regions of the detector, separated by ∼75 pixels. Results from standard processed data and wavelength corrected data are shown in black and gray, respectively. In most areas of the detector, the cross-correlation results of the corrected data are significantly flatter and closer to zero. Note that corrections derived from Capella and applied to V4743 Sgr data also improve observed non-linearities.

tracks deposited on a ceramic subtract (Murray et al. 1989). Every eighth wire or track is connected to a charge-sensitive amplifier (also known as a "tap"). Charge cloud positions resulting from photon events are estimated by the distribution of charge seen by the nearest three taps. However, this "three tap algorithm" leads to signal gaps in images half-way between taps. The "de-gap" correction adjusts the event positions to fill in the gaps and is implemented in standard processing.

The HRC-S degap forms the topic of a related paper, where it is described in detail (Kashyap et al. 2005). Future work needs to consider both the degap and wavelength non-linearities as coupled problems that are best approached iteratively. In this way, wavelength non-linearities would be mapped out as described here, then applied to events used to determine the parameters entering into the degap correction. The revised degap map would then be used in a new estimate of the wavelength distortions. Such an iterative approach is currently under development and will be reported in a future article.

5. ACKNOWLEDGEMENTS

This work was supported by NASA contracts NAS8-03060 and NAS8-39073 to the chandra X-Ray Center.

REFERENCES

1. A. Brinkman et al.," First Light Measurements of Capella with the Low-Energy Transmission Grating Spectrometer aboard the Chandra X-Ray Observatory " *ApJ* **530**, pp. L111-L114, 2000
2. S. Chung et al.,"Characterizing nonlinearities in the Chandra LETG+HRC-S Dispersion Relation" *Proc. SPIE*, pp. 518-529, Feb. 2004
3. J. Drake et al.,"Instruments: LETG" *Chandra newsletter* **Issue 11**, March 2003, http://cxc.harvard.edu/newsletters/news_11/letg.html
4. V. Kashyap et al.,"Chandra HRC-S Degapping Corrections" *Proc. SPIE*, 2005
5. S. Murray et al.," Position Modeling for the AXAF High resolution Camera (HRC)" *Proc. SPIE* **1159**, pp. 460-475, 1989
6. J. Schmitt et al.,"Simultaneous ORFEUS FUV and ROSAT X-ray observations of the young rapid rotator AB Doradus" *ApJ* **325**, pp. 249-254, 1997
7. M. Zombeck et al.," High-resolution camera (HRC) on the Advanced X-Ray Astrophysics Facility (AXAF) " *Proc. SPIE* **2518**, pp. 96-106, 1995